Grain size-dependent crystal plasticity constitutive model for polycrystal materials

Masoud Ghorbani Moghaddam, Ajit Achuthan*
Department of Mechanical and Aeronautical Engineering, Clarkson University, Potsdam, NY-13676
Brett A Bednarcyk, Steven M Arnold, Evan J Pineda
NASA Glenn Research Center, OH 44135

Abstract: -

A new method to introduce grain size-dependence in classical crystal plasticity constitutive model is developed by considering the resistance to dislocation motion in the grain boundary influence region as equivalent to that of a work hardening. A general framework for the size-dependent constitutive model is derived by implementing this method on a core and mantle model. The work hardening, equivalent to grain boundary effect, is realized by introducing a fictitious, pre-existing, plastic strain grain boundary influence region (mantle) following the principles of classical crystal plasticity. This fictitious plastic strain, in effect, increases the yield strength and decreases the initial hardening coefficient of the grain. With the thickness of grain boundary influence region and the distribution of introduced plastic strain remaining the same, the grain boundary effect increased as the grain size becomes smaller. A simplified model that considers the grain boundary effect on a grain average sense is also developed under this general framework. Implementation of this general framework to the specific cases of crystal plasticity constitutive models is demonstrated by considering the case of power law flow rule and hyperbolic-secant hardening rule. Finally, the grain size-dependent constitutive model is validated by comparing the predicted stress-strain behavior of polycrystal samples with different average grain sizes under uniaxial loading with the experimental results.

Keywords: grain size-dependent constitutive model; crystal plasticity;

1.0 Introduction

Microstructural features and their sizes have significant effect on material deformation. Yield strength of a crystalline metallic material increases when its grain size becomes smaller according to the Hall-Petch

relationship [1,2]. Similarly, the yield strength of nickel based superalloys increases with decrease in the average size of the precipitate phase for a given volume fraction of the precipitate [3-5]. The grain size-dependent behavior is attributed to the influence of grain boundaries on dislocation nucleation and its mobility; thus affecting plastic shear flow and hardening in slip systems. In classical crystal plasticity constitutive models [6-13], plastic deformation of a material is captured through a set of flow rule and strength evolution rule that describes the slipping deformation in the slip systems driven by resolved shear stress. However, these constitutive models do not have an intrinsic mechanism to capture the localized deformation influenced by microstructural features; therefore lack the ability to predict the experimentally observed feature size-dependent material behavior, such as grain size effect.

The mechanism of grain size-dependent behavior has also been explained as a consequence of the influence of strain gradients on material response, arising primarily due to lattice incompatibilities associated with the inhomogeneous plastic deformation between neighboring grains [14]. Accordingly, deformation gradient based constitutive models that fundamentally rely on dislocation density as an internal variable to capture the evolution of dislocations, were advanced by accounting for strain gradient effects [15-36]. Dislocations are generally classified into statistically stored dislocations (SSDs) that evolve from the random trapping processes during plastic deformation [15], and geometrically necessary dislocations (GNDs) that evolve as a result of the geometrical constraints on crystal lattice. Plastic strain gradients in materials are correlated to the evolution of GNDs that maintains lattice compatibility [16-19]. While a number of these studies used phenomenological models under the mathematical framework of Cosserat–Koiter–Mindlin theories of higher order elasticity [20-26], others followed a more physically intuitive approach by directly introducing strain gradient effects in the evolutionary laws of internal slip system state variables [3-5, 27-36]. Although these models captured the grain size-dependent flow stress quite well, they lacked a fundamental mechanism in the formulation to capture the yield strength variation with grain size [34-37]. The formulation of these models also results in mesh sensitivity, which not only is a challenge

in the implementation of the method, but more importantly, raises concerns on the physical foundation of the formulation as well.

In an alternative approach, grain size-dependent constitutive models were developed by subdividing a grain into a core and a mantle configuration [37-41]. The mantle that surrounds the core represents a region influenced by the grain boundary due to its proximity, and is modeled to deform differently from the core that represents the inner volume of the grain. This approach is primarily motivated by the experimental determination of increased hardening in the grain boundary influenced region near grain boundaries [42-45]. Meyers et al. [37] modeled grain as a composite of a work-hardened boundary layer (mantle) surrounding the grain interior comprised of an annealed material (core), in a polycrystalline aggregate. Model predicted an initial strengthening as expected. It was also shown that the flow stress of the aggregate can be obtained from the average of the flow stress in the dislocation free grain interior regions and the grain boundary influenced regions by applying a rule similar to the rule of mixture. Fu et al. [38] advanced this model by allowing for the evolution of dislocation density in the mantle, thus extending the model into the nano-crystalline regime. While the grain interiors were modeled using a limited form of crystal plasticity, the grain boundary influence regions were modeled using an isotropic plasticity model with a higher strain-hardening rate through evolution of dislocation density. The model was further advanced by incorporating the slip and rotation in the grain-boundary influence region [39]. Classical crystal plasticity model was applied to each of the core and mantle regions. To facilitate relatively easier dislocation generation and its mobility in the grain boundary region, a lower yield stress along with a higher work hardening rate were assigned to the mantle. Grain size-dependent behavior has also been modeled on the core and mantle framework by coupling the single-crystal plasticity constitutive model with an appropriate cohesive interface model [40, 41].

When compared to the deformation gradient based models, the core and mantle based models can capture the dependence of yield strength on grain size, and are relatively easy to implement. However, none of the core and mantle based models reported in the literature follow a grain size-dependent formulation in its true

sense. In these models, the grain size-dependent behavior is realized by applying the grain size independent classical constitutive models to the core and mantle separately with two different sets of material properties.

In the present study, a simple method to introduce grain size effect into the crystal plasticity constitutive model is developed on the core and mantle framework. The method fundamentally relies on introducing a strain-hardening in the grain boundary influence region, through a fictitious, pre-existing, distribution of a plastic strain so chosen that the resulting distribution of the resistance to dislocation nucleation and its mobility in that region is equivalent to the grain boundary effect. The main advantages of this new method are: 1) follows a better representation of the mechanism of grain boundary effect since grain size-dependence is realized by considering the resistance to dislocation nucleation and mobility more realistically in the formulation, 2) implementation of the fictitious pre-existing plastic strain in the grain boundary region follows the classical crystal plasticity constitutive model framework closely and requires only a minor modification to the classical crystal plasticity constitutive model framework, and 3) spatial distribution of the resistance to shear flow is the only additional information required. Examples that illustrate the capabilities of the new approach and demonstrate its ability to capture the Hall-Petch effect are presented. A simple linear profile for the fictitious plastic shear strain distribution in the grain boundary influence region is considered for numerical demonstration of the method, and the results are compared with those available in the literature.

2.0 Theory

A general framework for the grain size-dependent constitutive model is developed in section 2.1. The general framework is then simplified by considering the grain boundary effect on a grain average in section 2.2. Finally, the implementation of the general framework into specific cases of classical crystal plasticity constitutive models to obtain grain size-dependent constitutive model is demonstrated for the case of classical power law flow rule and hyperbolic-secant hardening behavior in section 2.3.

2.1 General Framework

Following the classical approach, the kinematics of elastic-plastic deformation is split into two multiplicative operations; a plastic deformation, where material is deformed through the rearrangement of lattices without any lattice stretching, followed by an elastic deformation associated with the stretching of lattices [17-21]. The total deformation gradient $\boldsymbol{F}$ is then given by,

$$\boldsymbol{F} = \boldsymbol{F^e}.\ \boldsymbol{F^p} \quad (1)$$

where $\boldsymbol{F^p}$ and $\boldsymbol{F^e}$ are the plastic and elastic deformation gradients, respectively.

The total velocity gradient $\boldsymbol{L}$ is given as,

$$\boldsymbol{L} = \boldsymbol{L}^* + \boldsymbol{L^p} = \dot{\boldsymbol{F}}.\boldsymbol{F^{-1}} = \boldsymbol{D} + \boldsymbol{\Omega} \quad (2)$$

where the symmetric stretch rate $\boldsymbol{D}$ and the anti-symmetric spin tensor $\boldsymbol{\Omega}$ can be decomposed into elastic $(\ \ )^*$ and plastic $(\ \ )^p$ parts,

$$\boldsymbol{D} = \boldsymbol{D}^* + \boldsymbol{D^p} \quad , \ \boldsymbol{\Omega} = \boldsymbol{\Omega}^* + \boldsymbol{\Omega^p} \quad (3)$$

The velocity gradient associated with the plastic deformation $\boldsymbol{L^p}$ is then given in terms of Schmid's tensor as,

$$\boldsymbol{L^p} = \boldsymbol{F^p}.\dot{\boldsymbol{F}}^{\boldsymbol{p}^{-1}} = \sum_\alpha \dot{\gamma}^{(\alpha)}\, \boldsymbol{m}^{(\boldsymbol{\alpha})} \otimes \boldsymbol{n}^{(\boldsymbol{\alpha})} \quad (4)$$

where $\dot{\gamma}^{(\alpha)}$ is the rate of shear strain associated with the slipping in α-th slip system, $\boldsymbol{m}$ is the unit normal to the slip plane, and $\boldsymbol{n}$ is the unit vector parallel to the slip direction. Incremental formulation of plasticity theory is based on; (1) evolution of Cauchy stress on a corotational frame of reference that rotates with the crystal lattice, $\boldsymbol{J}^*(\boldsymbol{\sigma})$, (2) shear flow rate (slipping rate) $\dot{\gamma}^{(\alpha)}$, and (3) strain hardening rate $\dot{g}^{(\alpha)}$ as given below,

$$\boldsymbol{J}^*(\boldsymbol{\sigma}) + \boldsymbol{\sigma}(\boldsymbol{I}{:}\,\boldsymbol{D}^*) = \boldsymbol{C}{:}\,\boldsymbol{D}^*, \quad (5)$$

where $\boldsymbol{\sigma}$ is the Cauchy stress and $\boldsymbol{C}$ is the tensor of elastic moduli.

The rate of slipping on a given slip system α is then defined as,

$$\dot{\gamma}^{(\alpha)} = \dot{\gamma}^{(\alpha)}\left(\tau^{(\alpha)}, g^{(\alpha)}\right) \tag{6}$$

where $\tau^{(\alpha)}$ and $g^{(\alpha)}$ are the resolved shear stress and the shear strength, respectively. Likewise, the evolution of strength in a given slip system α due to strain-hardening can be described as a function of the cumulative shear strain and the rate of shear flow in each of the slip systems as given below,

$$\dot{g}^{(\alpha)} = \sum_{(\beta)} h_{\alpha\beta}(\gamma)\, \dot{\gamma}^{(\beta)} \tag{7}$$

where $h_{\alpha\beta}$, a function of the cumulative shear strain γ, is the slip hardening moduli, and $\dot{\gamma}$ is the rate of shear flow. The sum ranges over all the slip systems. The coefficient $h_{\alpha\beta}$ represents the self-hardening modulus when $\alpha = \beta$, and the latent-hardening modulus otherwise. The cumulative shear strain γ is defined as,

$$\gamma = \sum_{(\alpha)} \int_0^t \left|\dot{\gamma}^{(\alpha)}\right| dt \tag{8}$$

The instantaneous shear strength of a slip system is then obtained as,

$$g^{(\alpha)} = \tau_0 + \int_0^t \dot{g}^{(\alpha)}\, dt \tag{9}$$

The resistance to dislocation nucleation and mobility near a grain boundary is attributed to the piling up of dislocations in the grain boundary influence region driven by the difference in grain orientation across the grain boundaries. Hence, a grain size-dependent constitutive model should incorporate a mechanism to capture this resistance to shear flow in the vicinity of the grain boundary. In the present study, we extended the basic framework of classical crystal plasticity constitutive model by considering a non-uniform distribution for the initial strength g, such that it includes an additional strength g_{GB} equivalent to the grain boundary resistance in the grain boundary influence region. Consequently, the strength evolution rule in the crystal plasticity constitutive model requires the introduction of a cumulative shear flow distribution $\tilde{\gamma}_{GB}$, corresponding to this additional strength distributiong_{GB}, since the hardening coefficient that determines the ability of the material for further evolution of strength is a function of the cumulative shear flow. It is important to note that the $\tilde{\gamma}_{GB}$is a fictitious quantity (indicated by the tilde symbol), introduced

simply to account for the change in hardening coefficient in the crystal plasticity constitutive model, unlike g_{GB} which is a real measure of the resistance to dislocation nucleation and mobility in the grain boundary influence region. Hence, a direct implementation of the method involves the determination of an appropriate distribution for g_{GB} first, followed by the determination of corresponding $\tilde{\gamma}_{GB}$ from g_{GB}. However, the determination of $\tilde{\gamma}_{GB}$ from g_{GB} under a crystal plasticity framework is quite cumbersome. Therefore, an alternative approach, more consistent with the crystal plasticity constitutive framework, is adopted. In this approach, a distribution for the fictitious cumulative shear flow $\tilde{\gamma}_{GB}$ is considered first, such that the g_{GB} obtained from $\tilde{\gamma}_{GB}$ using the evolution rule for strength is equal to the actual distribution of the grain boundary resistance.

The method is illustrated as follows. First, for a grain the fictitious cumulative shear flow distribution $\tilde{\gamma}_{GB}$ is introduced as a pre-existing strain in the grain boundary influence region of thickness (δ_{GB}) (Fig. 1).

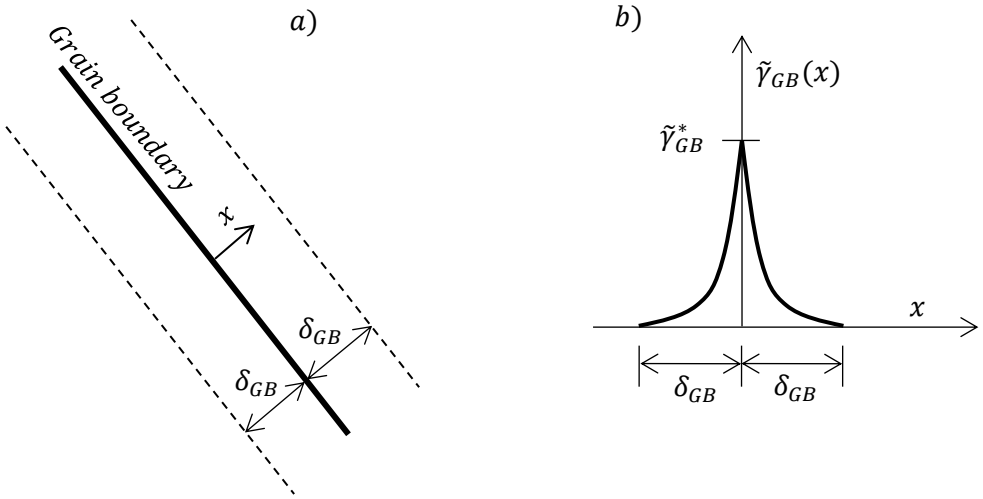

Figure 1 *(a) A schematic illustrating the grain boundary influence region (b) distribution of the fictitious pre-existing plastic shear strain*

$$\tilde{\gamma}_{GB} = \tilde{\gamma}_{GB}(x, \tilde{\gamma}^*_{GB}) \tag{10}$$

In the above equation x represents the distance from the grain boundary. The actual profile of $\tilde{\gamma}_{GB}$ depends on the grain boundary mechanism that is targeted, and could lead to strengthening or softening as grain size

decreases. Without loss of generality, in Figure 1(b) we considered a profile that increases in strength as the distance from the grain boundary decreases, reaching a maximum value of $\tilde{\gamma}_{GB}^{*}$ at the grain boundary. The distribution of this plastic pre-strain $\tilde{\gamma}_{GB}$ in the grain boundary influence region should be such that the distribution of the resulting strength (g_{GB}) must be equal to the actual resistance due to grain boundary effect, with a maximum resistance of g_{GB}^{*} at the grain boundary, and decreasing to the value of an annealed large grain as it approaches to the core. In general, g_{GB} (*i.e.* g_{GB}^{*}, δ_{GB}, and the profile) is a characteristic of the grain boundary, and should vary with the location on the grain boundary depending on many factors such as relative orientation of the grains across the grain boundary at that location. However, in view of simplicity, g_{GB} is treated in the present study as a material property that remains constant everywhere on the grain boundary of a given grain, as well as for all the grains. g_{GB}^{*}, in particular, is taken as the strength corresponding to a fully strain-hardened grain.

In order to formulate the size-dependent constitutive model following the proposed method, the hardening rule that describes the rate of shear strength evolution (Eqn. 7) and the instantaneous shear strength (Eqn. 9) are modified as,

$$\dot{g}^{(\alpha)} = \dot{g}^{(\alpha)}\left(\gamma + \tilde{\gamma}_{GB}, \dot{\gamma}^{(\beta)}\right) \tag{11}$$

$$g^{(\alpha)}(x) = \tau_{0\infty} + {g_{GB}}^{\alpha}(x) + \int_0^t \dot{g}^{(\alpha)}(x)\, dt \tag{12}$$

where the subscript ∞ indicates that the related quantity corresponds to a large grain sample, thus not influenced by the grain boundary. The strength ${g_{GB}}^{\alpha}(x)$ being a material property can be determined before the material is subjected to loading. The determination of ${g_{GB}}^{\alpha}(x)$ from $\tilde{\gamma}_{GB}$follows the crystal plasticity constitutive model framework, taking into account the fact that $\tilde{\gamma}_{GB}$ is fictitious, as discussed below.

The key assumption in the ongoing development of the constitutive model is that the resistance to shear flow in the grain boundary influence region can be treated similar to the resistance due to strain hardening. Consequently, the strength evolution rate in a given slip system (α) can be considered as a linear combination of the rate of shear flow in all the slip systems. Therefore,

$$\dot{g}_{GB}{}^{(\alpha)}(x) = \sum_{(\beta)} h_{\alpha\beta}(\tilde{\gamma})\, \dot{\tilde{\gamma}}^{(\beta)} \tag{13}$$

The increase in strength $g_{GB}{}^{\alpha}(x)$ can be determined from the above rate equation as,

$$g_{GB}{}^{\alpha}(x) = \int_0^{\tilde{t}_{GB}} \sum_{(\beta)} h_{\alpha\beta}(\tilde{\gamma})\, \dot{\tilde{\gamma}}^{(\beta)}\ dt \tag{14}$$

where the upper limit of time integration, $\tilde{t}_{GB}$, represents the time of evolution of strength due to the grain boundary influence. Since the plastic strain $\tilde{\gamma}_{GB}$ introduced to capture the physical quantity g_{GB} under the crystal plasticity framework is a fictitious quantity, $\tilde{t}_{GB}$ does not have any physical significance. In other words, we seek the spatial distribution of a mathematical quantity $\tilde{\gamma}_{GB}$ that when formulated in the crystal plasticity modeling framework yields the realistic distribution of physical quantity g_{GB} in the grain boundary influence region. Therefore, the integration in the equation to determine strength due to grain boundary effect can be transformed from the time domain to the plastic pre-strain domain,

$$g_{GB}{}^{\alpha}(x) = \int_0^{\tilde{\gamma}_{GB}} \sum_{(\beta)} h_{\alpha\beta}(\tilde{\gamma})\, d\tilde{\gamma}^{(\beta)} \tag{15}$$

It is important to note that, for a given $\tilde{\gamma}_{GB}$ distribution, the determination of $g_{GB}{}^{\alpha}(x)$ is independent of the shear flow rule (Eqn. 6), consistent with the fact that the shear flow and its evoltuion are fictitious. The slip-hardening modulus $h_{\alpha\beta}$ is a material property in the crystal plasticity constitutive model.

Since the characterisitics of grain boundary influence region is treated as a constant, irrespective of the nature of grain boundary or the grains across it, $g_{GB}^{(\alpha)}$ can be expressed as g_{GB}, an average value over all the slip-systems, and the above expression can be further simplifed as,

$$g_{GB}(x) = \int_0^{\tilde{\gamma}_{GB}} h_s(\tilde{\gamma})\, d\tilde{\gamma} + \ (N_{ss} - 1) \int_0^{\tilde{\gamma}_{GB}} h_l(\tilde{\gamma})\, d\tilde{\gamma} \tag{16}$$

where N_{ss} is the total number of slip systems in a grain, h_s and h_l are the self and latent slip hardening moduli.

The $g_{GB}(x)$, in principle, can be determined experimentally. For example, the hardness profile determined on the cross-section of a sample containing large grains using a nanoindenter can potentially provide

information for the determination of $g_{GB}(x)$. In the absence of such detailed information, a linear profile with the maximum strength at the grain boundary set to the strength of a fully work-hardened sample may be a good approximation. The challenge is to determine an appropriate $\tilde{\gamma}_{GB}$ that when applied to Eqn. 15 produces a $g_{GB}(x)$ distribution matching the distribution of resistance to dislocation nucleation and mobility in the grain boundary influence region (Eqn. 16). While obtaining an analytical closed form solution for $\tilde{\gamma}_{GB}$ is possible in some cases, numerical methods are required in general depending on the functional form of $h_{\alpha\beta}$.

The above hardening rules (Eqns. 11, 12 and 16), along with the flow rules (Eqns. 6 and 8) together describe the grain size-dependent constitutive model for an appropriate distribution of $\tilde{\gamma}_{GB}$ defined in the grain boundary influence region. Being a fictitious quantity, $\tilde{\gamma}_{GB}$ does not have any direct influence on the shear strain evolved under a given loading history (Eqns. 6 and 8). In the grain boundary influence region, where the yield strength is larger and the hardening modulus is lower due to the grain boundary effect, the increase in yield strength is explicitly captured through g_{GB} as per Eqn. 16, while the decrease in the initial hardening modulus is implicitly captured through $\tilde{\gamma}_{GB}$ presented in the hardening evolution rule (Eqn. 16).

2.2 General Framework: Simple model based on a grain average sense

The hardening rules (Eqns. 11, 12 and 16) can be further simplified by considering the grain boundary effects on an average sense over the grain volume. Accordingly, the hardening rules are modified as follows,

$$\dot{g}^{(\alpha)} = \dot{g}^{(\alpha)} = \dot{g}^{(\alpha)}\left(\gamma + \overline{\tilde{\gamma}_{GB}}, \dot{\gamma}^{(\beta)}\right) \tag{17}$$

$$g^{(\alpha)} = \tau_{0L} + \overline{g_{GB}} + \int_0^t \dot{g}^{(\alpha)} dt \tag{18}$$

where $\overline{\tilde{\gamma}_{GB}}$ and $\overline{g_{GB}}$ are the grain averaged shear flow and grain averaged shear strength equivalent to the grain boundary effect, respectively. The $\overline{\tilde{\gamma}_{GB}}$ and $\overline{g_{GB}}$ can be estimated by considering a spherical grain of diameter *D* representing the effective size of an actual grain with a non-spherical shape (Fig. 2). In this

formulation, r represents the distance from center of the equivalent spherical grain. The $\overline{\tilde{\gamma}_{GB}}$, is determined by considering a uniform distribution of $\tilde{\gamma}_{GB}$ in the whole grain.

$$\overline{\tilde{\gamma}_{GB}} = \frac{\int_V \tilde{\gamma}_{GB}\ dV}{V} \tag{19}$$

where V is the volume of the grain. Therefore, by modifying the Eqn. 16, $\overline{g_{GB}}$ can be determined as,

$$\overline{g_{GB}} = \int_0^{\overline{\tilde{\gamma}_{GB}}} h_s(\tilde{\gamma})\, d\tilde{\gamma} + (N_{ss} - 1) \int_0^{\overline{\tilde{\gamma}_{GB}}} h_l(\tilde{\gamma})\, d\tilde{\gamma} \tag{20}$$

The $\overline{g_{GB}}$ is the additional shear strength due to the grain boundary effect that is uniform in the grain. It is equivalent to g_{GB} in terms of the total shear flow as per Eqn. 19.

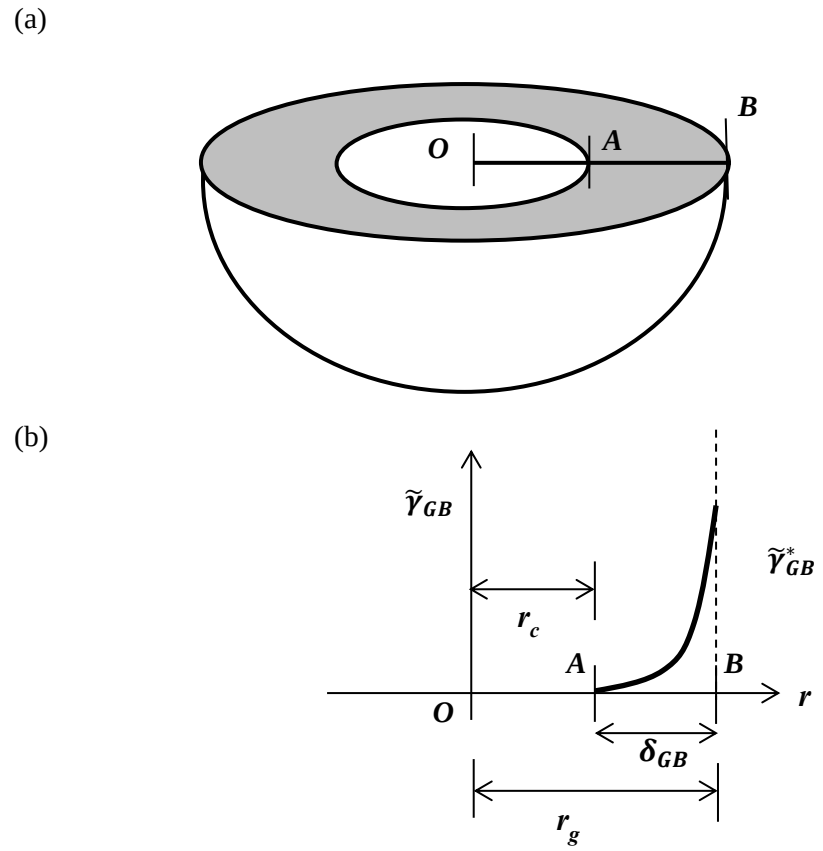

Figure 2 *(a) A schematic illustrating the grain boundary influence region by considering a simple spherical grain, (b) the distribution of a pre-existing shear strain equivalent to the resistance exerted by grain boundary.*

2.3 Implementation for specific cases

The general framework of the grain size-dependent constitutive model developed above based on a grain average sense is implemented for the special case of power law flow rule and hyperbolic-secant hardening behavior, widely reported in the literature [7-11]. A typical power law flow rule for the shear flow can be defined as

$$\dot{\gamma}^{(\alpha)} = \dot{a}\left(\frac{\tau^{(\alpha)}}{g^{(\alpha)}}\right)^{n} \tag{21}$$

where $\tau^{(\alpha)}$ and $g^{(\alpha)}$ are the resolved shear stress and the shear strength on the α-th slip system. The constant $\dot{a}$ refers to the slipping rate when resolved shear stress reaches the strength, and is assumed to be the same for all slip systems.

The coefficient $h_{\alpha\beta}$ (Eqn. 7) is defined as,

$$h_{\alpha\beta} = q^{(\alpha\beta)} h_0 sech^2\left|\frac{h_0\gamma}{\tau_s-\tau_0}\right| \tag{22}$$

where $q^{(\alpha\beta)}$ differentiates latent-hardening ($\alpha \neq \beta$) and self-hardening ($\alpha = \beta$), h_0 is the initial hardening modulus, τ_0 is the shear strength which is equal to the initial value of $g^{(\alpha)}$, and τ_s is the stage-I stress (break-through stress). Substituting the flow rule and the hardening rule (Eqns. 21 and 22) along with the $\tilde{\gamma}_{GB}$ (Eqn. 10) into Eqn. 16, $g_{GB}(r)$ can be obtained as,

$$g_{GB}(r) = \frac{\tilde{h}_{0\infty}}{K} tanh|K\tilde{\gamma}_{GB}(r)| \tag{23}$$

where the constants $\tilde{h}_{0\infty}$ and K are given as $\tilde{h}_{0\infty} = \frac{h_{0\infty}\left((N_{ss}-1)q+1\right)}{N_{ss}}$ and $K = \frac{h_{0\infty}}{\tau_s-\tau_{0\infty}}$, respectively, with N_{ss} being the total number of slip systems. The parameter $q^{(\alpha\beta)}$ is the same for all the $(N_{ss}-1)$ latent hardening slip systems (referred simply as q), and it is equal to one for the self-hardening slip system. From the grain averaged shear strain $\overline{\tilde{\gamma}_{GB}}$ (Eqn. 19), the grain averaged shear strength $\overline{g_{GB}}$ can be determined by substituting Eqns. 21 and 22 into Eqn. 20,

$$\overline{g_{GB}} = \tilde{h}_{0\infty} \int_0^{\tilde{\gamma}_{GB}} sech^2|K\tilde{\gamma}|\, d\tilde{\gamma} = \frac{\tilde{h}_{0\infty}}{K}\, tanh|\, K\overline{\tilde{\gamma}_{GB}}| \tag{24}$$

A simple linear profile for $\tilde{\gamma}_{GB}$ is considered as below,

$$\tilde{\gamma}_{GB}(r)=H(r-r_c)C\,(r-r_c) \tag{25}$$

where the constant C is given as $C = \frac{\tilde{\gamma}^*_{GB}}{\delta_{GB}}$ and the radius of the core r_c can be obtained by $r_c = r_g - \delta_{GB}$ with r_g being the radius of the equivalent spherical grain. $H(r-r_c)$ is the Heaviside step function enforcing value of 0 to the $\tilde{\gamma}_{GB}(r)$ profile for $r \le r_c$. $\overline{\tilde{\gamma}_{GB}}$ and $\overline{g_{GB}}$ are then determined as,

$$\overline{\tilde{\gamma}_{GB}} = \frac{\int_0^{r_g} |\tilde{\gamma}^*_{GB}(r)|4\pi r^2 dr}{\frac{4}{3}\pi(r_g)^3} = \tilde{\gamma}^*_{GB}\left(\left(\frac{3\delta_{GB}}{2r_g}\right) - \left(\frac{\delta_{GB}}{r_g}\right)^2 + \frac{1}{4}\left(\frac{\delta_{GB}}{r_g}\right)^3\right) \tag{26}$$

$$\overline{g_{GB}} = \tilde{h}_{0\infty} \int_0^{\tilde{\gamma}_{GB}} sech^2|K\tilde{\gamma}|\, d\tilde{\gamma} = \frac{\tilde{h}_{0\infty}}{K}\, tanh\left|K\tilde{\gamma}^*_{GB}\left(\left(\frac{3\delta_{GB}}{2r_g}\right) - \left(\frac{\delta_{GB}}{r_g}\right)^2 + \frac{1}{4}\left(\frac{\delta_{GB}}{r_g}\right)^3\right)\right| \tag{27}$$

3.0 Results and Discussion

The grain size-dependent constitutive model was validated by: 1) studying the variation of $\overline{g_{GB}}$ with grain size for an assumed linear profile for $\tilde{\gamma}_{GB}(r)$ (Eqn. 27) and verifying the Hall-Petch effect, and 2) incorporating the gran size-dependent constitutive model (Eqns. 6, 8, 17, and 18) on a finite element analysis (FEA) framework, and then comparing the predicted stress-strain behavior of the samples with different average grain sizes under uniaxial tensile loading to the corresponding experimental results reported in the literature.

Two different polycrystalline configurations, each consisting of 125 grains, and one with regular cubic grains of uniform size while the other with a more realistic case of grains with random shapes and sizes, were considered as representative volume elements (RVEs) (Fig. 2). The polycrystal configuration with random shapes and sizes were generated using Voronoi algorithm. Consideration of the two different RVEs in this study was aimed to determine whether the RVE with regular cubic grains, a widely used configuration in the literature [35, 36], is a realistic grain structure representation for obtaining the elasto-

plastic material behavior, especially when a grain size-dependent constitutive model is used. Experimentally obtained stress-strain behavior for copper samples with different average grain diameters of 14 μm, 33 μm and 220 μm is available in literature [47, 48]. In addition, the stress-strain behavior for the large grain (grain size-independent) sample was reported in a later study [48] obtained by extrapolating the experimental stress-strain behavior of these three different grain sizes. To compare the predicted results from the developed model in this article with experimental results, samples with the same average grain sizes (D_{ave}), namely 14 μm, 33 μm, and 220 μm, were considered for the simulation. The different average grain sizes were obtained by simply scaling the overall sample size, thus making sure that the grain shapes and orientations (Fig. 3) remained the same between sample to sample.

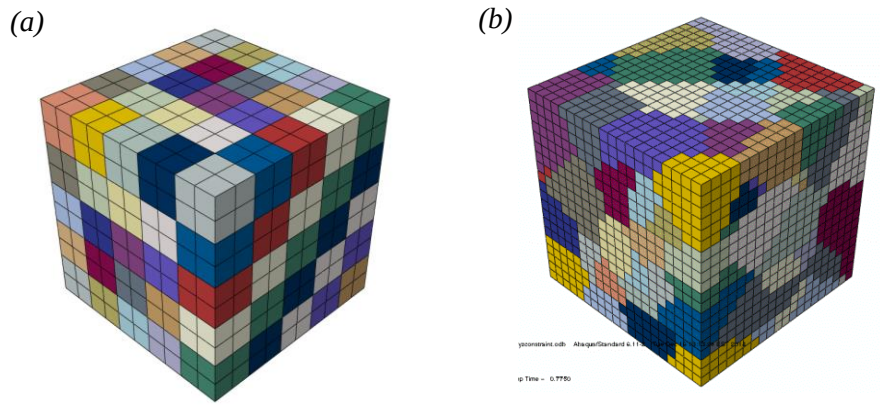

Figure 3 *Polycrystal with 125 randomly oriented grains (a) Cubic uniform grains, (b) random shape and size grains*

Since the material properties that describe plasticity were not available, an FEA simulation with a grain size-independent constitutive model (Eqns. 6-9) was performed first to derive these material properties. The plastic material properties τ_{oL}, τ_s, and h_{oL} were derived by matching the stress-strain behavior from the simulation with the stress-strain behavior estimated for the sample with large average grains (Table 1). The elastic material properties C_{11}, C_{12}, and C_{44}, for the copper cubic structure and the plastic material

parameters $\dot{a}_o$ and q were obtained from literature [46]. A relatively high value of 100 was considered for *n* in order to obtain a rate-independent flow rule.

Table 1 *Applied elastic and plastic material properties.*

Material Properties	
$\boldsymbol{\tau_{0L}}$	$9\ MPa$
$\boldsymbol{\tau_s}$	$95\ MPa$
$\boldsymbol{h_{0L}}$	$240\ MPa$
$\boldsymbol{\dot{a}_o}$	$0.001\ 1/s$
$\boldsymbol{n}$	100
$\boldsymbol{q}$	1
$\boldsymbol{\widetilde{\gamma}^*_{GB}}$	1.07
$\boldsymbol{c_{11}}$	$168400\ MPa$
$\boldsymbol{c_{12}}$	$121400\ MPa$
$\boldsymbol{c_{44}}$	$75400\ MPa$

Abaqus commercial FEA package with the crystal plasticity constitutive model, implemented through a UMAT subroutine, was used for both the grain size-independent simulation to derive material properties and the grain size-dependent study to validate the newly developed constitutive model. Sample was subjected to a uniaxial tensile load at a loading rate of 350 MPa/s. Periodic boundary conditions were enforced on all the external faces of the RVEs [35, 36]. For the polycrystal with cubic grains, each grain was discretized into a 2x2x2 mesh with 20-noded cubic brick elements as shown in Fig. 3a. Thus, each element assumes same size equal to $1/8^{th}$ of the size of the grain. The discretization of the sample with randomly shaped grains obtained using the voronoi algorithm is shown in Fig. 3b. In order to ensure a good refinement, even with respect to the smallest grain size, a 20x20x20 mesh of 20-noded brick elements was considered. Same uniaxial loading condition, boundary conditions and mesh refinement were used for the validation of grain size-dependent constitutive model.

The linear $\tilde{\gamma}_{GB}(r)$ profile given in Eqn. 25 was used for the validation of the grain size-dependent constitutive model. The maximum value for the fictitious cumulative shear flow $\tilde{\gamma}^*_{GB}$ was determined as 1.07 based on the cumulative shear flow corresponding to τ_s from the size-independent simulation. The $\overline{\tilde{\gamma}_{GB}}$, $g_{GB}\,(r)$, and $\overline{g_{GB}}$ for individual grains in both the cubic and random configurations were

determined following Eqns. 26, 23 and 27, respectively. A grain boundary thickness (δ_{GB}) of 0.33 μm was used in this study since it provided the best fit for the predicted stress-strain behavior with the experimental results for all the three samples with different average grain size.

3.1 Variation of $\overline{\tilde{\gamma}_{GB}}$, $g_{GB}\,(r)$, and $\overline{g_{GB}}$ with grain size

For the assumed linear profile of $\tilde{\gamma}_{GB}(r)$, the distribution of $\overline{\tilde{\gamma}_{GB}}$, $g_{GB}\,(r)$ and $\overline{g_{GB}}$ within a grain for three individual grains of sizes 14 µm, 33 µm, and 220 µm are shown in Fig. 3 and Table 2. These grain sizes are equal to the average grain sizes of the three polycrystal samples considered in the validation step. The horizontal axis is taken as the radial distance from the center of the grain normalized by the grain radius. As expected, both the $\overline{\tilde{\gamma}_{GB}}$ and $\overline{g_{GB}}$ increased as the grain size decreased.

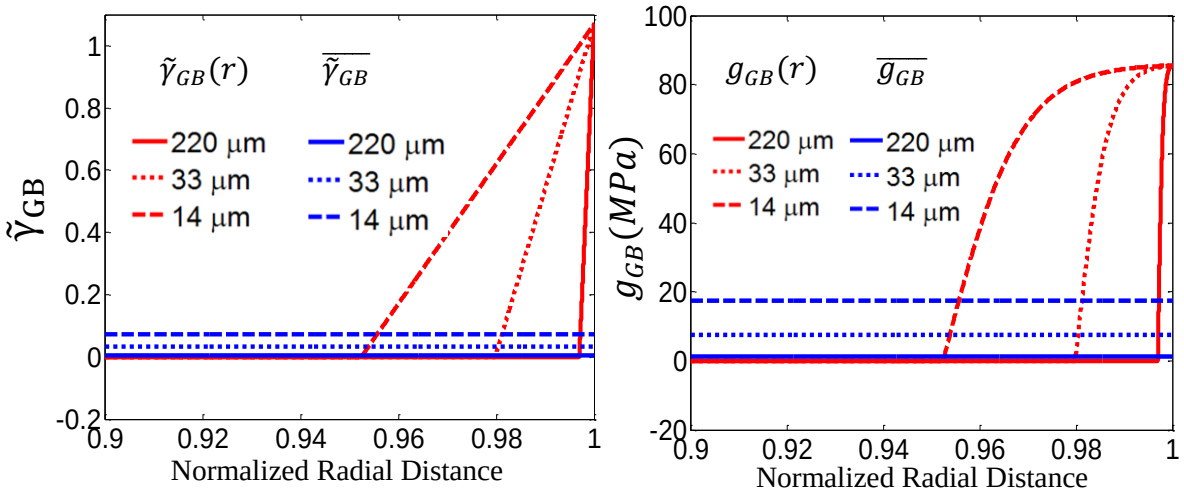

Figure 4 *(a) $\tilde{\gamma}_{GB}$ profile and the effective $\overline{\tilde{\gamma}_{GB}}$ $(horizontal\ lines)$ (b) g_{GB} profile and the effective $\overline{g_{GB}}$ $(horizontal\ lines)$*

Table 2 *$\overline{\tilde{\gamma}_{GB}}$ and $\overline{g_{GB}}$ for a single grain considering grain boundary effect*

$D_{grain}\ (\mu m)$	$\overline{\tilde{\gamma}_{GB}}$	$\overline{g_{GB}}\ (MPa)$
14	**0.0740**	**17.5000**
33	**0.0325**	**7.6495**
220	**0.0048**	**1.1637**

In the cubic configuration, the size of all grains being the same, the entire 125 grains have a constant diameter for their equivalent spherical grain representations (Fig. 2), and hence the $\overline{\tilde{\gamma}_{GB}}$, $g_{GB}\ (r)$, and $\overline{g_{GB}}$ for all of these grains are equal to the corresponding values calculated for the individual grain (Fig. 4 and Table 2).

The distributions of the grain size in the Vornoi polycrystal grain configuration is shown in Fig. 5, while the variations of $\overline{\tilde{\gamma}_{GB}}$, and $\overline{g_{GB}}$ with grain size are shown in Fig. 6. In the Voronoi polycrystal configuration, since the diameter of the equivalent spherical representation of each grain is different due to the difference in grain sizes, the values of $\overline{\tilde{\gamma}_{GB}}$ and $\overline{g_{GB}}$ vary from grain to grain. As the grain size increases the ratio of the volume of grain boundary influence region to the volume of grain decreases, thus decreasing the effect of the grain boundary resistance $\overline{g_{GB}}$. For the case of sample with the smallest average size, $14\ \mu m$, $\overline{g_{GB}}$ varies from 29.03 *MPa* for the smallest grain to 13.02 *MPa* for the largest, when compared to 17.50 *MPa*

obtained for the cubic grain. It should be noted that the value of $\overline{g_{GB}}$ for a given grain represents the addition in strength on a grain average sense in that grain as a result of the grain boundary effect.

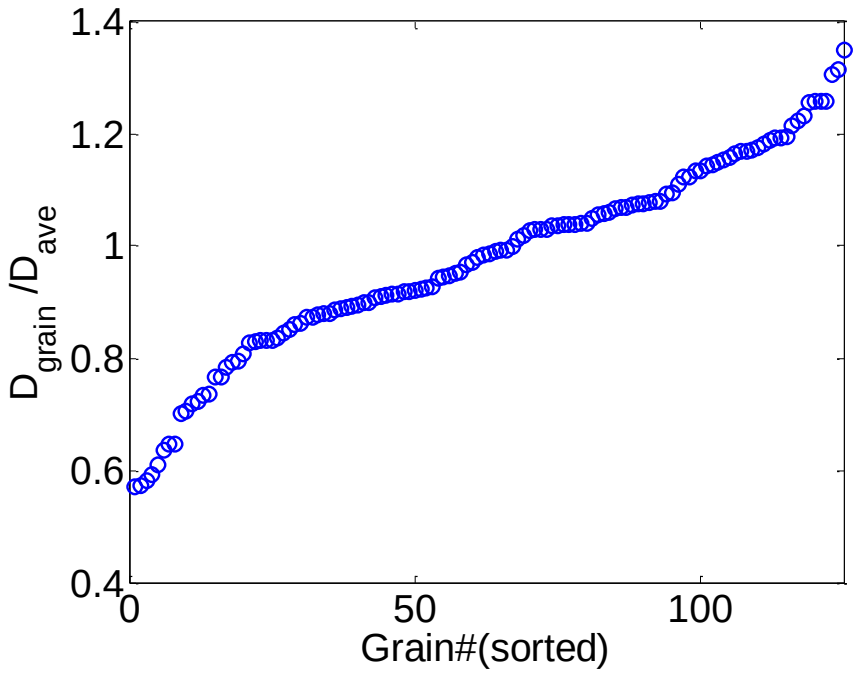

Figure 5 *The variation of the grain diameters normalized with the average grain diameter in the Voronoi polycrystal configuration for 125 grains. Since the three samples with different average grain sizes are obtained by simply scaling the geometry this variation is same for all of them*

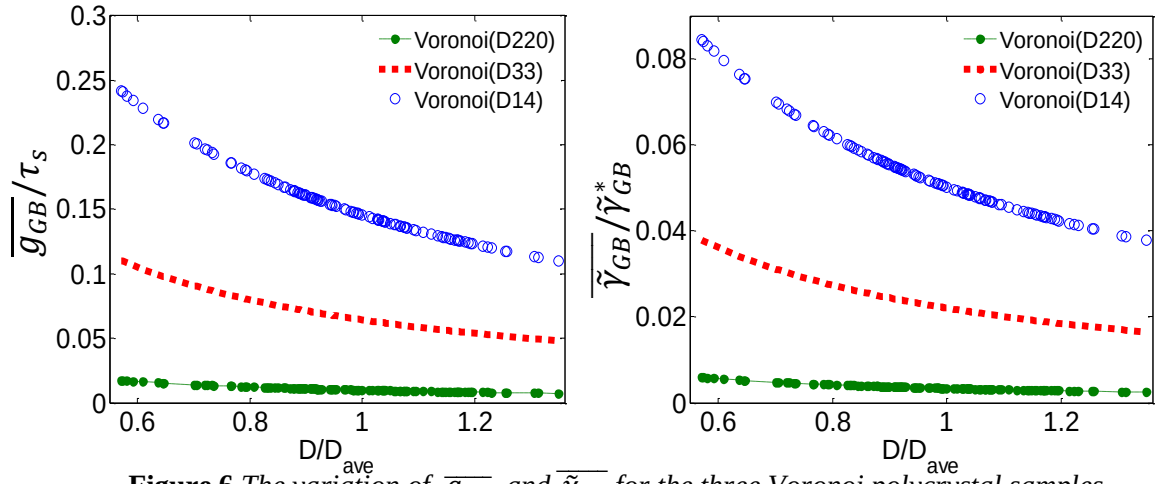

Figure 6 *The variation of* $\overline{g_{GB}}$ *and* $\overline{\tilde{\gamma}_{GB}}$ *for the three Voronoi polycrystal samples with different average grain sizes a) the variation in* $\overline{g_{GB}}$ *normalized by* τ_s *b) the variation in* $\overline{\tilde{\gamma}_{GB}}$ *normalized by* $\tilde{\gamma}^*_{GB}$

The Hall-Petch relation is verified for the range of grain sizes in the Voronoi polycrystalline sample (Fig. 7) by plotting the variations in the $\overline{g_{GB}}$ normalized by the $\overline{g_{GB}}$ of an individual grain of size equal to the average grain size (Table 2) against $\frac{1}{\sqrt{D}}$ normalized by the corresponding $\frac{1}{\sqrt{D_{ave}}}$.. The R^2 values for the linear fit for each of the cases demonstrated excellent matching with the expected behavior. In addition, the slopes for all the three cases considered were relatively close agreeing with the Hall-Petch effect.

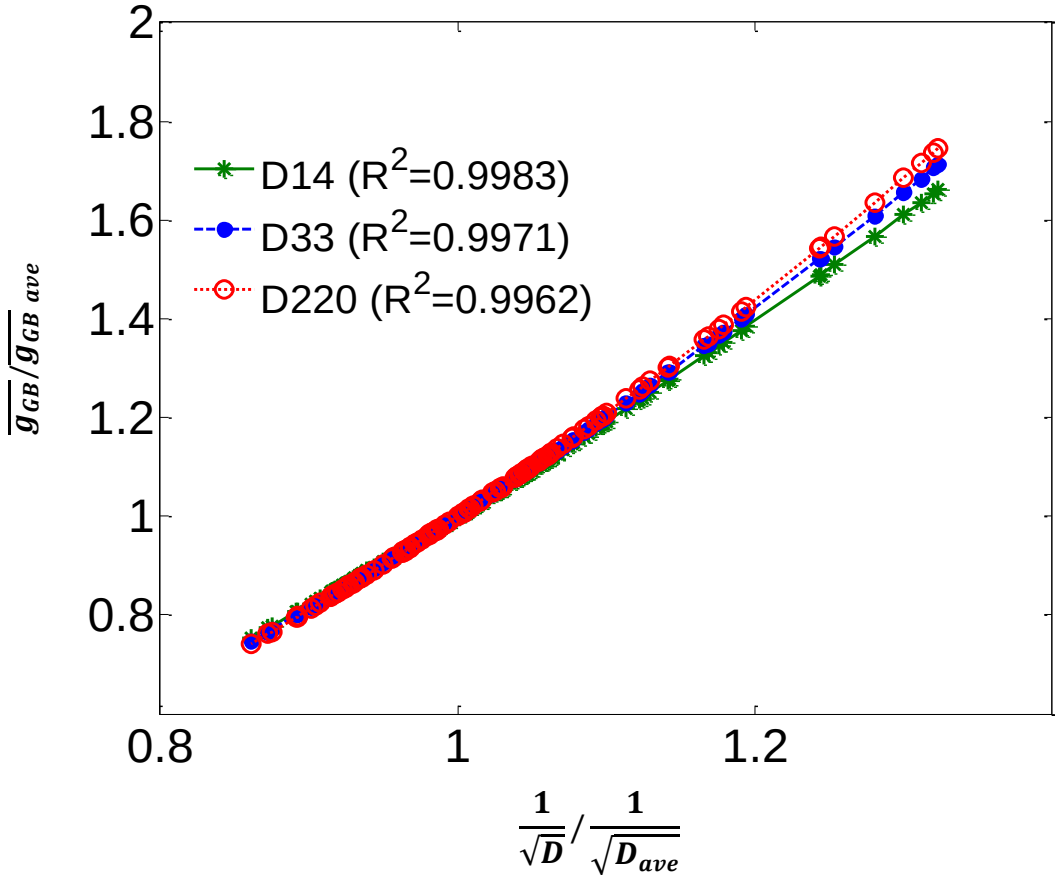

Figure 7 *Verification of the Hall-Petch relationship for the three Voronoi polycrystal configuration samples with average grain diameters of* 14 *μm*, 33 *μm and* 220 *μm.* R^2 *represents the regression coefficient related to the linear fit (* $\overline{g_{GB}}_{ave}$ *values reported in Table 2)*

3.2 Grain size-dependent constitutive model

In this section, validation of the grain size-dependent constitutive model (Eqns. 6, 8, 17, and 18) to capture the size-dependent stress-strain behavior is discussed. The values of $\overline{\tilde{\gamma}_{GB}}$ and $\overline{g_{GB}}$, obtained as functions of the grain size (discussed in the previous section), were assigned to individual elements in the finite element mesh as a material parameter in addition to the elastic and plastic material properties provided in Table 1. All the elements belonging to a given grain have the same values for $\overline{\tilde{\gamma}_{GB}}$ and $\overline{g_{GB}}$ calculated based on the corresponding equivalent spherical grain. In the case of Voronoi polycrystal configuration, the elements

that overlap between two grains in the grain boundary region were associated with one of the grains based on the location of the element's centroid.

The average axial stress-strain response for both the cubic grain polycrystal and the Voronoi polycrystal predicted by the FEA simulation using the grain size-dependent constitutive model are compared with the experimental results in Fig. 8. Overall, the predicted results agree very well with the experimental results. Though the experimental data is not sufficiently dense near the yield strength for an accurate comparison, the predicted increase in yield stress with decrease in grain size shows a clear trend that matches the expected behavior. Since the experimental results were available only for three average grain sizes, the variation of the predicted yield strength of polycrystal samples were not compared against $\frac{1}{\sqrt{D}}$ to validate Hall-Petch. However, the increase in the predicted yield stress of polycrystal samples with decrease in grain size as evident in the stress-strain behavior (Fig. 8), in addition to the good agreement with the Hall-Petch rule based on individual grains as demonstrated in the previous section, validate the theoretical development of g_{GB} (Eqn. 23) and $\overline{g_{GB}}$ (Eqn. 27) following crystal plasticity framework. It also validates the main assumption behind the proposed method that the resistance to shear flow in the grain boundary region can be treated similar to the resistance due to strain hardening. The excellent agreement between the predicted and experimental hardening behavior (stress-strain behavior beyond yield strength) validates the ability of the proposed general constitutive framework (Eqns. 6, 8, 17, and 18) to capture size-dependent plastic behavior. It is important to note that the influence of grain boundary on hardening behavior is captured through the $\gamma + \overline{\tilde{\gamma}_{GB}}$ quantity in Eqn. 17. Therefore, $\overline{\tilde{\gamma}_{GB}}$, although fictitious, introduces the right initial hardening modulus.

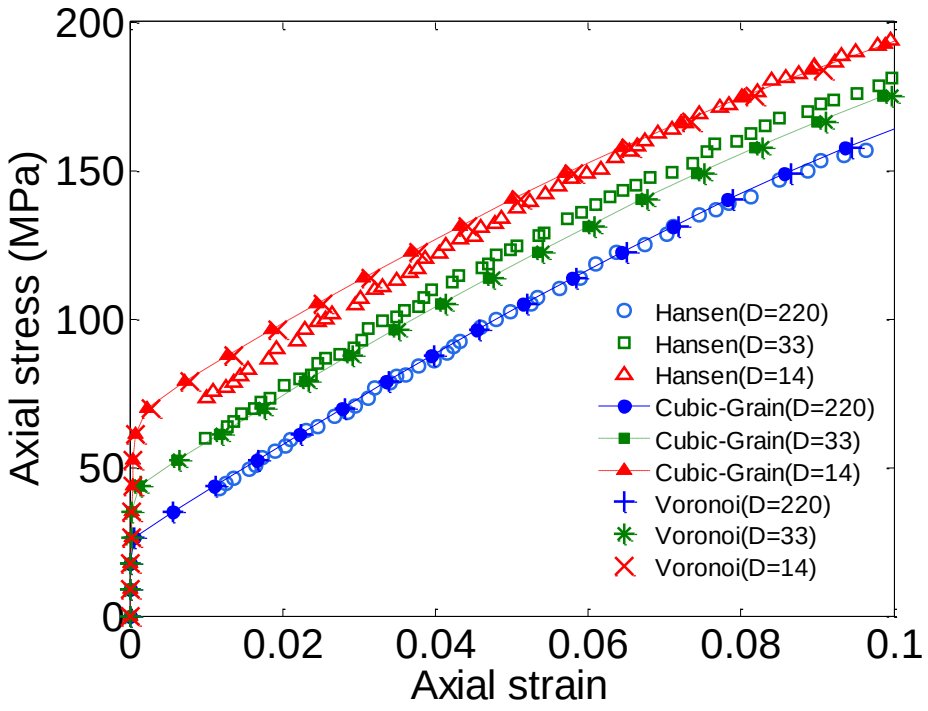

Figure 8 *Comparison of the axial stress-strain behavior obtained from the developed model for polycrystal with cubic grains and polycrystal by Voronoi grains with those from the Hansen experimental work [47, 48] for samples with grain diameters of* 14 *μm,* 33 *μm and* 220 *μm of* 14 *μm,* 33 *μm and* 220 *μm for a long strain range*

The excellent agreement between the results obtained from the cubic grain sample and the Voronoi grain sample also indicates, in terms of average response, that: 1) the 125 grains sample considered for this study is a satisfactory RVE for the polycrystalline material considered in this study, and 2) the effect of randomness in grain sizes and grain shapes is not significant, and hence the simple cubic grain sample widely used in the literature in general is a good representation of a polycrystal for obtaining size-dependent average stress-strain behavior.

In Fig. 8, the stress-strain behavior is shown only in the strain range of 0 to 0.1 due to the limited availability of the experimental data. In order to validate the model for a larger strain range, the axial stress-strain response predicted by the grain size-dependent model is shown for a larger strain range in Fig. 9. The variation of hardening modulus with grain size is quite evident in this depiction. For a given value of axial

strain (or axial stress) the slope of the curve representing the hardening modulus increases with increase in grain size [49].

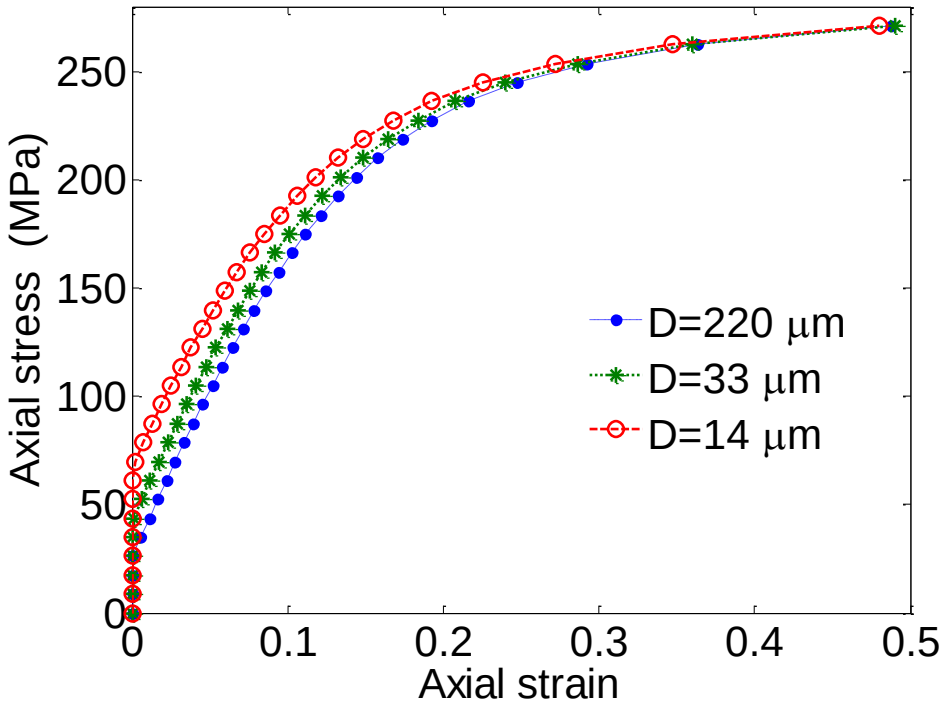

Figure 9 *Predicted size-dependent axial stress-strain behavior for Voronoi polycrystal configuration for a larger strain range*

4.0 Conclusion

A new simple method to introduce grain size dependence in the classical crystal plasticity constitutive model has been developed. Size dependence is realized by considering the resistance to dislocation motion in the grain boundary influence region as equivalent to a local strain-hardening, which was implemented in the constitutive model by introducing a fictitious pre-existing plastic strain. The model was validated by studying the variation of initial strength with grain size. Results showed increasing effect of grain boundary region in terms of increased initial strength and decreased hardening as the grain size decreased. The obtained solution demonstrated good agreement with the Hall-Petch theory. In addition, the size-dependent constitutive model was implemented on a FEA framework and the stress strain behavior of polycrystalline

samples comprised of 125 grains with three different average grain diameters of $14\ \mu m$, $33\ \mu m$ and $220\ \mu m$ sizes were obtained under uniaxial tensile loading. Comparison of predicted results with the experimental results available in literature revealed that a grain boundary influence region of $0.33\ \mu m$ thickness, with a linear pre-existing plastic strain profile can describe the size-dependent stress-strain behavior of the FCC copper polycrystalline samples. Two different types of polycrystal grain configuration, one with equal size cubic grains and the other with randomly shaped grains based on the Voronoi algorithm, both with randomly oriented grains, were used to study the grain size-effect. Results showed similar results indicating that both of these configurations adequately represent the size-dependent stress-strain behavior for these samples. In short, the proposed method provides a simple, physics based constitutive model to capture the size-dependent behavior of materials that can be quite beneficial in the stress and failure analysis of structural components at the microstructure length scale.

Acknowledgments

Author A. Achuthan would like to thank NASA Glenn Research Center and Ohio Aerospace Institute for the summer research fellowship grant that supported part of this work.

References

[1] Hall, E.O., 1951. The deformation and aging of mild steel: iii. discussion of results. Proceedings of the
Physical Society of London, Vol. B64, pp. 747–753
[2] Petch, N.J., 1953. The cleavage strength of polycrystals. J. Iron and Steel Institute 174, 25–28.
[3] Busso, E. P., Meissonnier, F. T., & O'dowd, N. P. (2000). Gradient-dependent deformation of two-phase single crystals. *Journal of the Mechanics and Physics of Solids*, *48*(11), 2333-2361.
[4] Meissonnier, F. T., Busso, E. P., & O'Dowd, N. P. (2001). Finite element implementation of a generalised non-local rate-dependent crystallographic formulation for finite strains. *International Journal of Plasticity*, *17*(4), 601-640.
[5] Tinga T, Brekelmans W A M and Geers M G D 2008 Incorporating strain-gradient effects in a multi-scale constitutive framework for nickel-based superalloys *Phil. Mag.* 88 3793–825
[66] G.I. Taylor, J. Ins. Metals 62, 307 (1938).

[7] R. Hill, J. Mech. Phys. Solids 14, 95 (1966).
[8] R. Hill, J. Mech. Phys. Solids 15, 79 (1967).
[9] R. Hill, J.R. Rice, J. Mech. Phys. Solids 15, 401(1972).
[10] D. Peirce, R.J. Asaro, A. Needleman, Acta. Metall. 30, l087 (1982).
[11] R. Asaro, Adv. Appl. Mech. 23, 1 (1983a).
[12] Kalidindi, S.R., Bronkhorst, C.A., Anand, L., 1992. Crystallographic texture evolution in bulk deformation processing of fcc metals. J. Mech. Phys. Solids 40, 537–569.
[13] Bronkhorst, C.A., Kalidindi, S.R. Anand, L., 1992. Polycrystalline plasticity and the evolution of crystallographic texture in FCC metals. Philosophical Transactions of the Royal Society of London A, Vol. 341, pp. 443–477.
[14] Fleck, N.A., Muller, G.M., Ashby, M.F., Hutchinson, J.W., 1994. Strain gradient plasticity: theory and experiment. Acta Metallurgica et Materialia 42, 475–487.
[15] Arsenlis, A., Parks, D.M., 1999. Crystallographic aspects of geometrically-necessary and statistically stored dislocation density. Acta Mater. 47, 1597–1611.
[16] Ashby, M.F., 1970. The deformation of plastically non-homogeneous materials. Philosophical Magazine 21, 399–424.
[17] Nye, J.F., 1953. Some geometrical relations in dislocated crystals. Acta Metall. 1, 153–162.
[18] Aifantis, E.C., 1987. The physics of plastic deformation. Internat. J. Plasticity 3, 211–247.
[19] Armstrong, R., Codd, I., Douthwaite, R.M., Petch, N.J., 1962. The plastic deformation of polycrystalline aggregates. Philosophical Magazine 8, 45–58.
[20] Fleck, N.A., Hutchinson, J.W., 1997. Strain gradient plasticity. Adv. Appl. Mech. 33, 295–361.
[21] Gurtin, M.E., 2003. On a framework for small deformation visco-plasticity: free energy, microforces, strain gradients. Int. J. Plasticity 19, 47–90.
[22] Gudmundson, P., 2004. A unified treatment of strain gradient plasticity. J. Mech. Phys. Solids 52, 1379– 1406.
[23] Fleck NA, Hutchinson JW. J Mech Phys Solids 1993;
[24] Mindlin RD. Arch Ration Mech Anal 1964;16:51.
[25] Koiter WT. Proc K Ned Akad Wet (B) 1964;67:17
[26] Toupin RA. Arch Ration Mech Anal 1962;11:385.
[27] Dai, H., 1997. Geometrically necessary dislocation density in continuum plasticity theory, FEM implementation and applications. Ph.D. Thesis, Massachusetts Institute of Technology, Department of
Mechanical Engineering.
[28] Dai, H., Parks, D.M., 1997. Geometrically necessary dislocation density and scale-dependent crystal plasticity. In: Khan, A.S. (Ed.), Proceedings of Plasticity '97: The Fifth International Symposium on Plasticity and its Current Applications. Neat Press, Juneau, Alaska, pp. 17–18.
[29] Arsenlis, A., Parks, D.M., 2000. Application of a three-dimensional model for plastic strain gradient crystal plasticity to grain-size dependent mechanical behavior of polycrystals, private communication.
[30] Arsenlis, A., Parks, D.M., 2001. Modeling the evolution of crystallographic dislocation density in crystal plasticity. J. Mech. Phys. Solids 50, 1979–2009.
[31] Busso, E.P., Cheong, K.S, 2001. Length scale effects on the macroscopic behaviour of single and polycrystalline FCC crystals. J. Phys. IV 11, Pr(5) 161–169.

[32] Cheong, K.S., Busso, E.P., 2004. Discrete dislocation density modeling of pure single-phase FCC crystals. Acta Mater. 52, 5665–5675.
[33] Bassani, J.L., 2001. Incompatibility and a simple gradient theory of plasticity. J. Mech. Phys. Solids 49, 1983–1996.
[34] Acharya, A., Bassani, J.L., 2000. Lattice incompatibility and a gradient theory of crystal plasticity. J.
Mech. Phys. Solids 48, 1565–1595.
[35] Evers, L. P., et al. "Crystal plasticity model with enhanced hardening by geometrically necessary dislocation accumulation." Journal of the Mechanics and Physics of Solids 50.11 (2002): 2403-2424.
[36] Cheong, K. S., Busso, E. P., & Arsenlis, A. (2005). A study of microstructural length scale effects on the behaviour of FCC polycrystals using strain gradient concepts. International Journal of Plasticity, 21(9), 1797-1814.
[37] M. A. Meyers, E. Ashworth, Phil. Mag. A. 46 (1982) 737.
[38] Fu, H., Benson, D.J., Meyers, M.A., 2001. Analytical and computational description of effect of grain size on yield stress of metals. Acta Mater. 49, 2567–2582.
[39] H.H. Fu, D.J. Benson, M.A. Meyers, Acta Mater. 52 (2004) 4413.
40] Y.J. Wei. L. Anand, J. Mech. Phys. Solids 52 (2004) 2587.
[41] Y. J. Wei, C. Su, L. Anand, Acta Mater. 54 (2006) 3177.
[42] Gray III, G.T., Chen, S.R., Vecchio, K.S., 1999. InHuence of grain size on the constitutive response and substructure evolution of MONEL 400. Metall. Mater. Trans. A 30, 1235–1247.
[43] Murr, L. E. and Hecker, S. S., Scripta metall., 1979, 13, 667.
[44] Suits, J. C. and Chalmers, B., Acta metall., 1961, 12, 854.
[45] Worthington, P. J. and Smith, E., Acta metall., 1964, 12, 1277.
[46] Y. Huang, A User-material Subroutine Incorporating Single Crystal Plasticity in the ABAQUS Finite Element Program. Harvard Univ., 1991.
[47] N. Hansen, Proc. 5th int. Conf. Strength of Metals and Alloys p. 849. Pergamon, Oxford, 1979.
[48] N. Hansen, B. Ralph, *Acta Metall* 30 (1982) 411
[49] N. Hansen, Scripta. Mater. 51, 801(2004).